High-speed polarization-resolved third-harmonic microscopy

Joséphine Morizet, Guillaume Ducourthial, Willy Supatto, Arthur Boutillon, Renaud Legouis, Marie-Claire Schanne-Klein, Chiara Stringari, Emmanuel Beaurepaire

▶ **To cite this version:**

Joséphine Morizet, Guillaume Ducourthial, Willy Supatto, Arthur Boutillon, Renaud Legouis, et al.. High-speed polarization-resolved third-harmonic microscopy. Optica, 2019, 6 (3), pp.385-388. 10.1364/OPTICA.6.000385 . hal-02114087

HAL Id: hal-02114087

https://polytechnique.hal.science/hal-02114087v1

Submitted on 16 Dec 2020

HAL is a multi-disciplinary open access archive for the deposit and dissemination of scientific research documents, whether they are published or not. The documents may come from teaching and research institutions in France or abroad, or from public or private research centers.

L'archive ouverte pluridisciplinaire **HAL**, est destinée au dépôt et à la diffusion de documents scientifiques de niveau recherche, publiés ou non, émanant des établissements d'enseignement et de recherche français ou étrangers, des laboratoires publics ou privés.

Copyright

Letter Vol. 6, No. 3 / March 2019 / Optica 385

optica

High-speed polarization-resolved third-harmonic microscopy

Joséphine Morizet,[1] Guillaume Ducourthial,[1] Willy Supatto,[1] Arthur Boutillon,[1] Renaud Legouis,[2] Marie-Claire Schanne-Klein,[1] Chiara Stringari,[1,3] and Emmanuel Beaurepaire[1,4]

[1]Laboratoire d'Optique et Biosciences, Ecole polytechnique, CNRS, INSERM, 91128 Palaiseau, France
[2]Institute for Integrative Biology of the Cell (I2BC), CEA, CNRS, Univ. Paris-Sud, Université Paris-Saclay, 91198, Gif-sur-Yvette, France
[3]e-mail: chiara.stringari@polytechnique.edu
[4]e-mail: emmanuel.beaurepaire@polytechnique.edu

Received 29 August 2018; revised 29 January 2019; accepted 28 February 2019 (Doc. ID 344581); published 19 March 2019

Polarization-resolved third-harmonic generation (P-THG) is a sensitive probe of material anisotropy and molecular ordering. Despite its promises, this property has little been used in biological tissues due to the lack of measurement schemes compatible with dynamic samples. We report here on the development of a fast P-THG microscope where excitation polarization is switched between line scans using an electro-optic modulator, providing temporal resolution in the 10 ms range for the polarimetric measurement. We demonstrate novel applications enabled by this approach, associated with Fourier-based analysis: probing molecular order in deforming lipid structures undergoing phase transition; revealing crystallinity of flowing particles in the zebrafish embryo's inner ear; and detecting birefringence *in vivo*. These results establish that P-THG is ideally suited for probing lipid organization and mineralization in dynamic biological environments. © 2019 Optical Society of America under the terms of the OSA Open Access Publishing Agreement

https://doi.org/10.1364/OPTICA.6.000385

Since its first demonstrations, third-harmonic generation (THG) microscopy [1] has emerged as an effective imaging modality for the label-free characterization of interfaces in cells and tissues, with applications ranging from cell and developmental biology to neuroscience [2–4]. The contrast mechanism of THG microscopy is somewhat peculiar. When the excitation field is focused by a high numerical aperture (NA) microscope objective, THG efficiency is dominated by the Gouy phase shift, which prevents phase matching between the fundamental and harmonic fields over the focal region in the case of isotropic normally dispersive media. The consequences for THG microscopy images are that no signal is generally obtained from homogeneous regions and optical heterogeneities at the micrometer or sub-micrometer scale are highlighted over a dark background. Lipid-water interfaces or cell-derived vesicles [3–5], for example, are readily visualized. This contrast permits label-free structural imaging of intact tissue with three-dimensional sectioning. THG imaging is also directly compatible with widely used multiphoton microscopy modalities such as fluorescence and second-harmonic generation, to which it can provide an informative morphological context [2,4–6].

A less used property of THG microscopy is its dependence on the driving field polarization when probing anisotropic media [Figs. 1(a)–1(b)]. One first remarkable characteristic is that no TH polarization is induced in an isotropic medium excited with a circular polarization, owing to $\chi^{(3)}$ tensor symmetries [7–9]; see Fig. 1(a). Therefore, the comparison of THG images obtained with linear (L-THG) and circular (C-THG) polarization provides a means to detect anisotropic media [8,10]. Furthermore, in birefringent media, THG signals can be obtained even from homogeneous regions if birefringence is strong enough to compensate the phase mismatch caused by the Gouy shift [8]. Moreover, THG from an anisotropic medium excited by a linearly polarized beam strongly depends on the angle between the driving polarization and the medium optical axes [Fig. 1(b)]. For example, at the surface of a multilamellar lipidic structure parallel to the propagation axis [Fig. 1(c)], the THG intensity variation as the incident polarization is rotated by 180° can be described as a single-peaked response in the form $I(\Phi) = A + B\cos(\Phi - \Phi_0)^2$, where B depends on molecular ordering, and Φ_0 depends on mean molecular orientation [11]. Inside a strongly birefringent medium such as a liquid crystal [Fig. 1(d)], this variation takes the double-peaked form $I(\Phi) = A + B\cos(\Phi - \Phi_0)^4 \sin(\Phi - \Phi_0)^2$, where Φ_0 depends on crystalline axes and on the type of phase matching involved [12].

The dependence of THG on incident polarization is therefore a probe of birefringence and molecular ordering. Despite its promises, this property has little been used for biological imaging beyond proofs of principle [8,10,11,13–15] up until now. The main reason is that probing the THG polarization dependence requires the recording of signals with several excitation polarization states while the sample is moving or deforming. We report here on the development of a fast polarization-resolved THG (P-THG) microscope where excitation polarization is switched within microseconds between every line scan using an electro-optic modulator [16,17], combined with a Fourier-based analysis method of the polarization data for identifying the different types of THG signals. We demonstrate three measurements enabled by

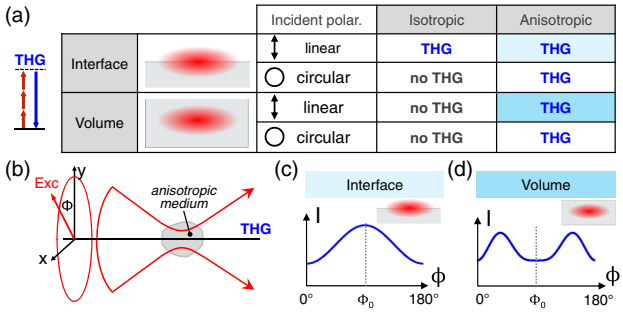

Fig. 1. Contrast mechanisms in P-THG microscopy. (a) Possibility of THG in isotropic and anisotropic materials depending on sample geometry and incident polarization. The red spot represents the beam focus. (b)–(d) Typical P-THG intensity profiles from (c) the interface or (d) the volume of an anisotropic material.

fast P-THG microscopy: (i) probing molecular order in deforming multilamellar lipid structures undergoing phase transition; (ii) revealing biomineralization of flowing particles in the highly dynamic environment of the zebrafish embryo's inner ear; and (iii) one-shot detection of birefringence from ordered lipids and biocrystals in live organisms.

We implemented our fast P-THG method [Fig. 2(a)] on a custom-built point-scanning multiphoton microscope integrating a femtosecond laser source (80 MHz, 1100 nm, 100 fs, Insight DS+, SpectraPhysics), galvanometric scanners (GSI Lumonics,

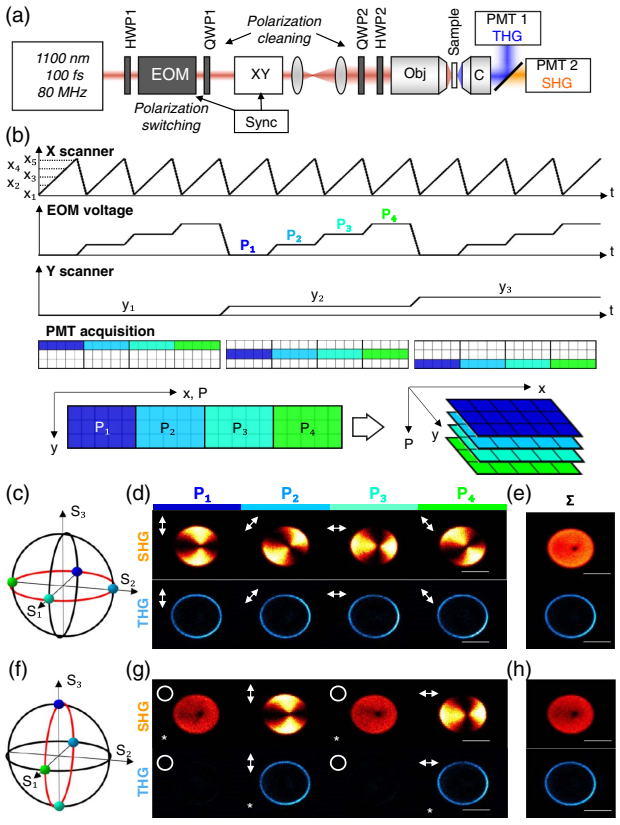

Fig. 2. EOM-based P-THG. (a) Experimental setup. (b) Sequence of scanning and EOM signals for XPY acquisition. (c)–(h) Simultaneous P-SHG and P-THG imaging of a starch granule while switching between linear polarization states (c)–(e) and horizontal/circular states (f)–(h). (e)–(h) Average of individual polarization images. (c)–(f) Polarization states shown on Poincaré sphere. Scale bar 10 μm.

USA), and a water immersion objective (25× , 1.05 NA, Olympus, Japan). Harmonic light detection was performed in transmission using a high-NA condenser (Olympus), filters (Semrock FF01-550/49 for SHG and FF01-377/50 for THG), photon-counting detectors (SensTech, UK), and lab-designed MHz-rate-counting electronics. Scanning, polarization control, and acquisition were synchronized using LabVIEW-written software and an I/O board (National Instruments, USA). Signal level was typically 20–80 photons/pixel with 5–10 μs/pixel and 40–150 mW excitation. Following previous works on fast polarization-resolved nonlinear imaging [16–18], we designed an alternative strategy consisting of scanning each line several times with different polarization states. This approach provides an interesting compromise between simplicity (hence robustness) and speed (temporal resolution in the millisecond range), and was not previously explored for THG imaging. The critical feature to implement was a polarization switching scheme operating in the sub-ms range [Fig. 2(b)] while maintaining good polarization purity at focus (Fig. S1). We achieved polarization state switching in less than 12 μs using an electro-optic modulator (EOM) driven by a high-voltage amplifier (350–150 and 302 RM, Conoptics, Connecticut, USA) and set between a half-wave plate (HWP1) and a quarter-wave plate (QWP1) [16] [Fig. 2(a)]. This configuration enables two polarization switching modalities, corresponding to rotating along either the equator or a meridian of the Poincaré sphere [Figs. 2(c) and 2(f)]. The first modality results in a linear polarization rotating in the plane transverse to the propagation axis [Figs. 2(c)–2(e)], and the second modality provides alternating linear and circular polarizations [Figs. 2(f)–2(h)]. Selecting one modality can be done by a 45° rotation of the QWP. We introduced an additional QWP (QWP2) at the entrance pupil of the objective in order to compensate for the polarization distortions caused by the microscope optics and the scanning system [Fig. 2(a)]. By iteratively adjusting the two QWPs' orientations for a series of voltage set points, we obtained an ellipticity $\sqrt{I_{\min}/I_{\max}}$ less than 0.08 for all incident linear polarizations [Figs. S1(a)–S1(b)] and >0.99 for circular polarizations [Fig. S1(c)]. We recorded all images over a 150 × 150 μm^2 region where artifactual angular shifts were less than 2° [Fig. S1(d)]. A second HWP (HWP2) was also inserted for convenient control of the polarization reference. X-P-Y acquisition was implemented by synchronizing galvanometer scanning and EOM voltage control, as shown in Fig. 2(b) and Visualization 1. A P-series of N images corresponding to N polarization states can then be reconstructed from the data [Fig. 2(b)]. The temporal resolution of the polarimetric analysis is here the time needed to record N lines, i.e., a few milliseconds: in the typical case of a line consisting of 400 pixels including scan flyback and with 5 μs pixel dwell time, it takes 8 ms to probe four polarization states or 36 ms to probe 18 polarization states. Figures 2(d)–2(h) illustrate the two acquisition modes described above. Here, THG and second-harmonic generation (SHG) polarization-resolved images of a starch granule are recorded simultaneously on two channels. Figures 2(c)–2(e) illustrate P-images where a linear polarization is rotated by 45° steps, and Figs. 2(f)–2(h) illustrate switching between circular and linear polarizations.

We now discuss the possibilities offered by fast P-THG for probing dynamic processes. We recently reported that P-THG is sensitive to molecular order in lipid structures [11]. This capability comes from the fact that the third-order nonlinear susceptibility response of lipid molecules far from vibrational resonance is

dominated by the contribution of the aligned C-C bonds in the lipid tails. Multilamellar lipid vesicles (MLVs, or "lipid onions") are a good model of ordered molecular systems that can be probed using polarization-resolved nonlinear microscopy [11,18,19]. We recorded fast-P-THG images of 1,2-Dimyristoyl-sn-glycero-3-phosphorylcholine (DMPC, Avanti Polar Lipids, Alabama, USA) MLVs synthesized using the method described in [20] and Supplement 1 [Fig. 3(a) and Visualization 2]. Interestingly, since MLVs are birefringent, they produce THG through the two types of mechanisms discussed above: (i) heterogeneity-related THG is detected at the external lipid-solvent interface, and (ii) weaker THG signals resulting from birefringence-induced phase matching are recorded from the inner regions of the MLV. Signals recorded from the vesicle periphery and from inner regions therefore exhibit different polarization-resolved profiles [Fig. 3(a)]: the interface signal is maximized when the incident polarization is parallel to the C-C chains, i.e., perpendicular to the interface; in contrast, the birefringence-induced inner signals exhibit two maxima as the incident polarization is rotated by 180° [11,12]. To analyze such data, we developed a fit-free methodology relying on the calculation of the Fourier components of P-THG signals (FT-PTHG). As shown in Figs. 3(a)–3(b) and Fig. S2, interface signals are dominated by the first two Fourier components ($c_0 - c_1$), whereas birefringence-related signals are characterized by the additional presence of $c_2 - c_3$ components. FT-PTHG therefore provides a means to identify and analyze the two types of THG signals. We automatically calculated binary masks [Fig. 3(c)] selecting either interface- or birefringence-related THG by thresholding r-squared-based maps of the difference between raw data and reconstructions based on relevant Fourier orders (i.e., $c_0 + c_1$ for interface signals and $c_0 + c_2 + c_3$ for birefringence-related signals). We then extracted average lipid orientation at the pixel scale in both regions based on the phase of the first-order terms [Figs. 3(c) and S2].

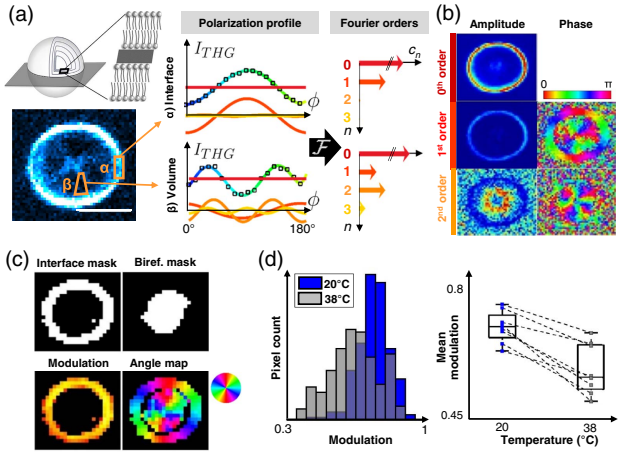

Fig. 3. Probing molecular order with Fourier analysis of P-THG data. (a) THG image of multilamellar lipid vesicle (MLV) from an 18-image P-THG sequence recorded with rotating linear polarizations. See Visualization 2. Scale bar 5 μm. Also shown are examples of polarization profiles and Fourier coefficients for interface and birefringence-related THG signals. (b) FT maps of the first three Fourier coefficients. (c) Masks, P-THG modulation, and molecular angle maps extracted from the data. (d) Decrease of the interface P-THG modulation amplitude measured in MLVs undergoing phase transition under heating. Left, pixel modulation histogram for a single vesicle. Right, pooled data from eight vesicles.

More importantly, we remind the reader that the modulation amplitude of interface P-THG signals $(I_{max} - I_{min})/I_{max} = 4c_1/(c_0 + 2c_1)$ is in MLVs a probe of molecular ordering [11]. We therefore used fast FT-PTHG to follow molecular disordering upon vesicle heating, and successfully monitored P-THG lipid order decrease in MLVs undergoing partial phase transition when heated from 20°C to 38°C [Fig. 3(d)]. Despite the fact that vesicles imaged at 38° exhibited deformations during imaging time at the sub-second scale, our acquisition scheme produced accurate modulation maps, revealing lipid disordering with sub-μm spatial resolution.

We then explored the possibility to detect biomineralization in a dynamic 3D environment using fast P-THG by analyzing the early stages of otolith formation in wild-type zebrafish embryos (see Supplement 1). The otolith is a mineralized structure involved in gravity sensing that grows under constrained biochemical conditions inside a cavity of the inner ear [Fig. 4(a)]. It is principally made of aragonite, a crystalline form of calcium carbonate. The initial stage of otolith growth is characterized by the transient presence in the cavity of precursor microparticles (or "spherules" [21]) of unknown nature, which move at speeds in the 1–50 μm/s range in a cilia-driven flow [21]. We found that both the forming otolith and these microparticles produce readily detectable THG signals in live embryos [Fig. 4(b), Visualization 3]. We then used fast P-THG to determine whether the microparticles are made of anisotropic material. We recorded P-THG images of flowing microparticles and, as a control, of 1 μm fluorescent polystyrene beads microinjected in the inner ear cavity. We analyzed the image series by extracting histograms of THG modulation amplitude for both types of objects [Figs. 4(c)–4(d), Fig. S3]. These data reveal without ambiguity that the endogenous microparticles are of crystalline nature (36 ± 16% P-THG modulation), unlike the isotropic polystyrene beads (18 ± 8% P-THG modulation). This experiment demonstrates the potential of P-THG for monitoring biomineralization *in vivo*. The findings reported here are particularly illustrative, as the microparticles exhibit rapid 3D motion, can form only in their native biological environment, and cannot be easily labeled.

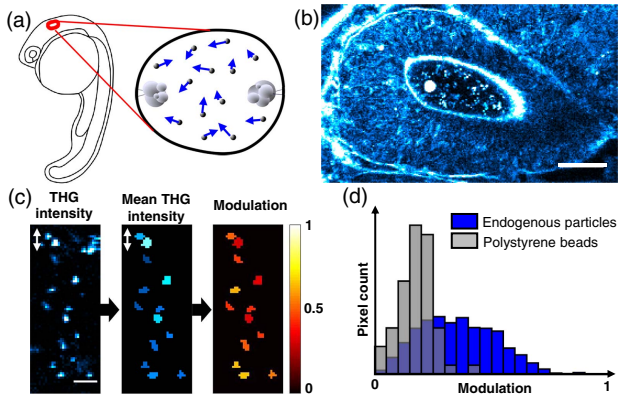

Fig. 4. *In vivo* detection of anisotropy of flowing microparticles in the zebrafish inner ear. (a) Schematic of the otic cavity in a 22 h post fertilization (hpf) zebrafish. (b) THG image of the cavity containing otolith precursor microparticles flowing at 1–50 μm/s. Scale bar 20 μm. See Visualization 3. (c) Extraction of the microparticles mean P-THG modulation. (d) Histogram of THG modulation for endogenous otolith microparticles (blue) and injected polystyrene beads (gray). The data identify that the microparticles are made of anisotropic material.

To demonstrate a final type of application of our method, we revisited an overlooked aspect of THG microscopy, which is that it provides a means to detect anisotropic materials by comparing images recorded with L-THG and C-THG incident polarization [8,10]. Our fast P-THG scheme provides a means to use this property in biologically relevant contexts by recording simultaneously the two images, in turn enabling ratiometric comparisons at the pixel scale. We implemented this idea by recording L-THG/C-THG image pairs in oil droplets, zebrafish otoliths *in vivo*, and MLVs [Figs. 5(a)–5(c)]. We used these data to derive an anisotropy parameter defined as C-THG/(L-THG+C-THG) [Figs. 5(d)–5(f)]. Oil droplets have isotropic molecular structure and produce no C-THG. We found that the growing larval otoliths exhibit strong P-THG modulation, like their precursor microparticles. Moreover, THG signals are obtained throughout the otolith with circular incident polarization, which is a signature of birefringence. Finally and as mentioned previously, MLVs exhibit both types of THG signals. As demonstrated in Figs. 5(g)–5(i), anisotropy parameter maps allow immediate identification of birefringence-related THG signals, with a threshold value around 17%. This provides a novel contrast strategy for label-free nonlinear microscopy. We applied this method to the detection of birefringent structures in live adult *C. elegans*. Intestinal cells of worms are densely packed with lipidic vesicles involved in metabolism. A fraction of these vesicles have been described as being birefringent, lysosome-related organelles [22]. THG observation of adult *C. elegans* worms provides detailed morphological images [23] where micrometer-sized vesicles in the intestine and epithelium are readily detected. We found that fast P-THG combined with anisotropy mapping identifies a fraction of these vesicles that do exhibit birefringence [Fig. 5(j)]. This contrast mechanism can therefore be exploited to identify structurally distinct intestinal stores *in vivo*.

In conclusion, we have described a methodology for fast polarization-resolved THG microcopy with millisecond temporal resolution on the polarimetric measurement. Our system can be used to perform a one-shot P-THG experiment where the incident polarization explores multiple states located along either the equator or a meridian of the Poincaré sphere, in turn probing either the molecular orientations or the $\chi^{(3)}$ tensor symmetries responsible for the P-THG response. We have shown that Fourier-based or ratiometric analyses of the polarization-resolved images obtained in this manner provide measurements uniquely suited for dynamically probing lipid molecular organization and/or biomineralization in biological environments such as unlabeled *C. elegans* worms and developing zebrafish embryos. These results establish a novel contrast modality for label-free nonlinear biomicroscopy.

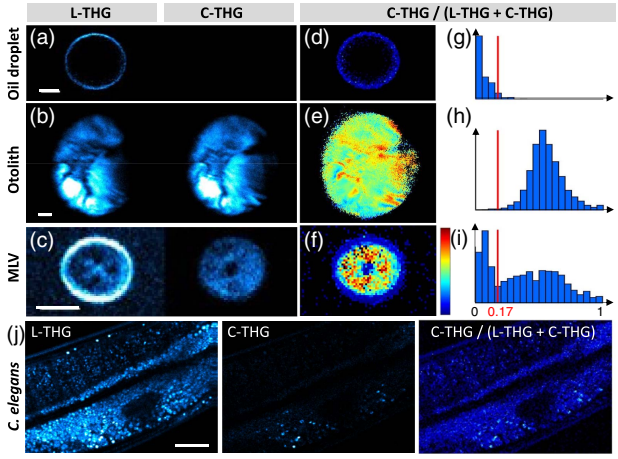

Fig. 5. Detection of birefringence with circular-linear polarization switching. (a)–(i) One-shot measurement of the anisotropy parameter C-THG/(L-THG+ C-THG) in an oil droplet (isotropic), a three-days zebrafish otolith (birefringent) and a MLV (both types of THG signals). Scale bars 5 μm. (j) Application: *in vivo* detection of birefringent granules in an adult *C. elegans* worm. Scale bar 20 μm.

Funding. Agence Nationale de la Recherche (ANR) (ANR-11-EQPX-0029, ANR-10-INBS-04, ANR-15-CE11-0012).

Acknowledgment. We thank Xavier Solinas for advice on electronics synchronization, Chrystel Faure for advice on MLV synthesis, Emilie Menant for zebrafish husbandry, Julien Vermot and Philippe Herbomel for discussion on zebrafish otolith formation, and Nicolas Olivier, Pierre Mahou, and Max Zimmerley for discussions on P-THG microscopy.

See Supplement 1 for supporting content.

REFERENCES

1. Y. Barad, H. Eisenberg, M. Horowitz, and Y. Silberberg, Appl. Phys. Lett. **70**, 922 (1997).
2. N. Olivier, M. A. Luengo-Oroz, L. Duloquin, E. Faure, T. Savy, I. Veilleux, X. Solinas, D. Débarre, P. Bourgine, A. Santos, N. Peyriéras, and E. Beaurepaire, Science **329**, 967 (2010).
3. M. J. Farrar, F. W. Wise, J. R. Fetcho, and C. B. Schaffer, Biophys. J. **100**, 1362 (2011).
4. B. Weigelin, G. J. Bakker, and P. Friedl, J. Cell Sci. **129**, 245 (2016).
5. D. Débarre, W. Supatto, A.-M. Pena, A. Fabre, T. Tordjmann, L. Combettes, M.-C. Schanne-Klein, and E. Beaurepaire, Nat. Methods **3**, 47 (2006).
6. N. Olivier, F. Aptel, K. Plamann, M.-C. Schanne-Klein, and E. Beaurepaire, Opt. Express **18**, 5028 (2010).
7. S. You, H. Tu, E. J. Chaney, Y. Sun, Y. Zhao, A. J. Bower, Y. Z. Liu, M. Marjanovic, S. Sinha, Y. Pu, and S. A. Boppart, Nat. Commun. **9**, 2125 (2018).
8. R. W. Boyd, *Nonlinear Optics* (2008).
9. D. Oron, E. Tal, and Y. Silberberg, Opt. Lett. **28**, 2315 (2003).
10. M. Samim, S. Krouglov, and V. Barzda, Phys. Rev. A **93**, 033839 (2016).
11. M. Zimmerley, P. Mahou, D. Débarre, M.-C. Schanne-Klein, and E. Beaurepaire, Phys. Rev. X **3**, 011002 (2013).
12. R. S. Pillai, M. Oh-e, H. Yokoyama, G. J. Brakenhoff, and M. Müller, Opt. Express **14**, 12976 (2006).
13. L. Kontenis, M. Samim, S. Krouglov, and V. Barzda, Opt. Express **25**, 13174 (2017).
14. G. Bautista, S. G. Pfisterer, M. J. Huttunen, S. Ranjan, K. Kanerva, E. Ikonen, and M. Kauranen, Biophys. J. **107**, 2230 (2014).
15. S. W. Chu, S. Y. Chen, G. W. Chern, T. H. Tsai, Y. C. Chen, B. L. Lin, and C. K. Sun, Biophys. J. **86**, 3914 (2004).
16. P. Stoller, K. M. Reiser, P. M. Celliers, and A. M. Rubenchik, Biophys. J. **82**, 3330 (2002).
17. E. L. Dewalt, S. Z. Sullivan, P. D. Schmitt, R. D. Muir, and G. J. Simpson, Anal. Chem. **86**, 8448 (2014).
18. M. Hofer, N. K. Balla, and S. Brasselet, Optica **4**, 795 (2017).
19. J. Cheng, S. Pautot, D. Weitz, and X. Xie, Proc. Natl. Acad. Sci. USA **100**, 9826 (2003).
20. A. D. Bangham, M. M. Standish, and J. C. Watkins, J. Mol. Biol. **13**, 238 (1965).
21. D. Wu, J. B. Freund, S. E. Fraser, and J. Vermot, Dev. Cell **20**, 271 (2011).
22. G. J. Hermann, L. K. Schroeder, C. A. Hieb, A. M. Kershner, B. M. Rabbitts, P. Fonarev, B. D. Grant, and J. R. Priess, Mol. Biol. Cell **16**, 3273 (2005).
23. G. J. Tserevelakis, E. V. Megalou, G. Filippidis, B. Petanidou, C. Fotakis, and N. Tavernarakis, PLoS One **9** e84431 (2014).